PARTICLE ACCELERATION IN MICROSTRUCTURES

A.A. Mikhailichenko
Wilson Laboratory, Cornell University, Ithaca, NY 14853

A device for charged particles acceleration described here, uses multi-cell microstructures aligned along the straight beam path. Each cell of these microstructures has an opening from the side. Focused laser radiation with appropriate wavelength excites the cells through these openings. This excitation is going locally in accordance with instant position of accelerated micro-bunch of particles in the structure. For this purpose special devices controllably sweep focused laser spot along the openings. This arrangement, what was called Travelling Laser Focus (TLF), reduces the instant power required from the laser source and reduces the illuminating time for the every point on the structure's surface. The power reduction and the shortening of illumination time equate to the *number of resolved spots* associated with the sweeping device. On practice, the number of resolved spots could reach 10-100 depending on the wavelength. Sweeping along the accelerating structure could be made about 3 *cm* long. Thus, the linac is sectioned with 3-*cm* long modules.

For a wavelength $\lambda_{ac} \cong 10\mu m$ a laser with energy 0.3*J/m* in 100*ps* pulse duration gives the gradient about 3 *GeV/m*. For example, a single flash with 300*J*, could provide the final energy of 3 *TeV* on 1 *km* with the TLF method described. Utilization of a laser radiation with $\lambda_{ac} \cong 1\mu m$ requires about hundred times smaller emittances, but ten times less particles and with the same laser power and accelerating length the final energy could reach ~30 *TeV*. Amplifiers distributed periodically along the linac could deliver this total power required as well. For repetition rate ~160 *Hz* the luminosity associated with colliding beams could reach $L \approx 10^{33} cm^{-2} s^{-1}$ per bunch with population ~10^6. Multi-bunch operation mode together with an increase of repetition rate up to *kHz* scale gives a reasonable value for the luminosity upgrade. Polarization is another important tool, which could be implemented here. Wall plug power required for operation of this linear collider could be as low as ~ *2 MW* for the parameters indicated above.

For 0.5×0.5*TeV* collider, the wall plug power required is ~330 *kW* and the length of collider is 2×170 *m* for $\lambda_{ac} \cong 10\mu m$. For $\lambda_{ac} \cong 1\mu m$ the length shrinks to 2×17 *m*. All components of this laser driven linac, including the source of low emittance beam are within present day technology.

Possible implementation for $\mu\mu$, $\pi\pi$, *pp* and *ion-ion* collisions mentioned also.

For details and references see: A.A. Mikhailichenko, *Particle acceleration in Microstructures, Excited by Laser Radiation,* CLNS 00/1662, Cornell, 2000.

1.WHY DO WE NEED A STRUCTURE?

The laser radiation is not able to accelerate particles in a vacuum.
Structure serves as housing for accelerating field.
The mostly important role of the structure is in *positioning* of accelerating field in 3D space.
Many projects on laser acceleration suffer from sensitivity to fluctuations in laser homogeneity.

Accuracy due to electron plasma in a metal is $\sim r_D/\lambda$, where Debye radius r_D defined as $r_D = \frac{v_p}{\omega_p} \cong \frac{\sqrt{k_B T/m}}{\omega_p} = \sqrt{\frac{k_B T}{4\pi n e^2}}$, where $k_B \cong 1.38\cdot 10^{-23}$ J/°K –is Boltzmann's constant, T –is electron temperature, n –is an electron density in a metal, r_0 –is a classical electron radius. Formally, as $\omega_p \cong 10^{16} 1/s$, $v_p \cong 10^8 cm/s$, $r_D \cong 10^{-8} cm$ and the ratio $r_D/\lambda \cong 10^{-4}$.

In diluted plasma with density $\sim 10^{-6}$ of density in metal, the last ratio becomes $r_D/\lambda \cong 10^{-1}$ only. In general, the plasma methods must experience problems with fluctuations of the number of electrons in Debye sphere $\Delta n \cong \sqrt{N_D}$. The last number is $N_D \cong \frac{4}{3} n r_D^3 \cong \frac{1}{\sqrt{n}}\left(\frac{k_B T}{4\pi e^2}\right)^{3/2}$ so $\Delta n \sim 1/\sqrt[4]{n}$.

Namely this makes stable acceleration in plasma problematic on the physical background.

Electromagnetic properties of metals at wavelengths: $\lambda_{ac} \approx 1-10\mu m$.

When the frequency of incoming radiation increases and comes to infrared region, the minimal among three dimensions: skin depth δ, free electron path in metal l_{free} and v_F/ω, where v_F –is the electron velocity at the Fermi surface, the last one becomes the smallest one. The mean free path of electrons at room temperature is $\sim 10^{-4} cm$. The time between collisions, hence $l_{free}/v_F \cong 10^{-12} s$. With decreasing temperature the last time drops $\sim 1/T^2$.

This is natural sequence of dependence $\delta\omega \sim \omega^{2/3}$ for anomalous region. What is important, that the energy of incoming laser radiation still lower than the Fermi energy E_F. Under these conditions the conductivity of the metal becomes imaginary

$$\sigma \cong \frac{i}{4\pi}\frac{\omega_p^2}{\omega} \quad .$$

(For typical metals $c/\omega_p \cong 10^{-5} cm$. For Copper at low temperatures the time corresponding to electron-imperfection collisions goes to $\sim 10^{-8} s$).

Electric field $E'' = -4\pi i\omega\sigma E/c^2$ becomes $E'' - (\omega_p^2/c^2)E = 0$ so $E \cong E_0 \exp(-\omega_p x/c)$ and the penetration depth is not a function of the frequency. The surface impedance $E/H \cong -i\omega/\omega_p$ is *fully imaginary*. This means that reflection of the laser wave from the surface is going *without dissipation*. This is a natural sequence of the assumption made: the electrons do not collide during the period of incoming radiation. Decreasing the temperature of the metal helps to reduce the dissipation as the *phonon* density decreases with temperature, as the time between electron phonon collisions drop $\sim 1/T$.

2. LIMIT FOR GRADIENT

Natural limit for the field strength emerges from requirement that the work done by electric field to the particle on the distance of Compton wavelength $\lambda\!\!\!^{-}_C = \hbar / mc$ is equal to the rest energy of electron-positron pair as $eE^{\infty}\lambda\!\!\!^{-}_C \cong 2mc^2$. The last gives the break down limit for a vacuum (So called Schwinger field)

$$E^{\infty} \cong \frac{2mc^2 / e}{\lambda\!\!\!^{-}_C} \ ,$$

what is $E^{\infty} \cong 1MV / 3.86 \cdot 10^{-13} m \cong 2.6 \cdot 10^{18}\ V / m$. Of cause, the breakdown limit in media is much lower.

Desire to have acceleration as high as possible brings the laser power close to the destruction limit for the materials an accelerator structure made on.

The latest measurements show a damage threshold increase while the illumination time is shortening. This breaks the $\tau^{1/2}$ low. This was explained by saturation of impact ionization rate per unit distance. Measured threshold for 0.3 *ps* pulse was about 10 J/cm^2. For 1 *ps* the threshold measured was 6 J/cm^2. In our case we have 10*mJ* laser pulse distributed over area 3×10^{-3} cm^2 what gives 3 J/cm^2 and accelerating gradient 3 *GeV/m*. We believe that these figures could be improved after careful preparation the surface and optimizing the working temperature and proper chose of material.

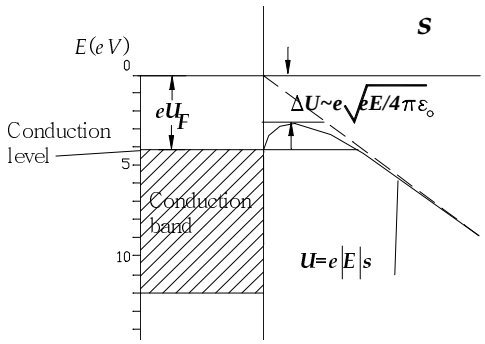

FIGURE 1: To the estimation of the limiting electrical field strength on the surface of metal.

The tunneling probability

$$D \approx \exp\left[-\frac{4\sqrt{2m}}{3\hbar eE}\left(eU_F - e\sqrt{eE}\right)^{3/2}\right], \text{ CGSE}$$

$$U_F \approx \sqrt{eE/(4\pi\varepsilon_0)} \ .$$

The last expression gives the estimation of the limiting field strength

$$E \approx \frac{4\pi\varepsilon_0 U_F^2}{e} \ .$$

Substitute here $U_F \approx 5V$, $\varepsilon_0 \cong \frac{1}{36\pi}10^{-9} F/m$, one can obtain $E \approx 17 GeV/m$.

3. THE TLF METHOD

Proper arrangement of excitation of accelerating structure of any kind becomes a crucial moment of all acceleration strategy.

It is naturally not to apply a laser power to the places of the structure, where there are no particles.

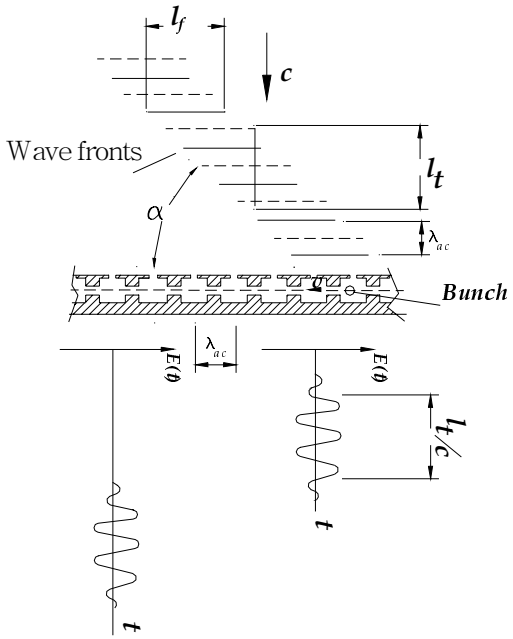

FIGURE 2: The concept of illumination. The time dependence of the field at two different locations along the structure is represented on the graphs at the bottom. Beam has a speed $\vec{v}$ to the left.

Traveling Laser Focus (TLF) method deals with a laser radiation focused onto a spot with minimal area. This spot ***sweeped*** in longitudinal direction as a function of time, following the particle in its motion along the accelerating structure. As the motion of the focused laser spot along the structure is going with the speed of particle.

With the TLF method, the power reduction and shortening of illuminating time is equal numerically to **the *number of resolved spots* (*pixels*),** associated with the sweeping device.

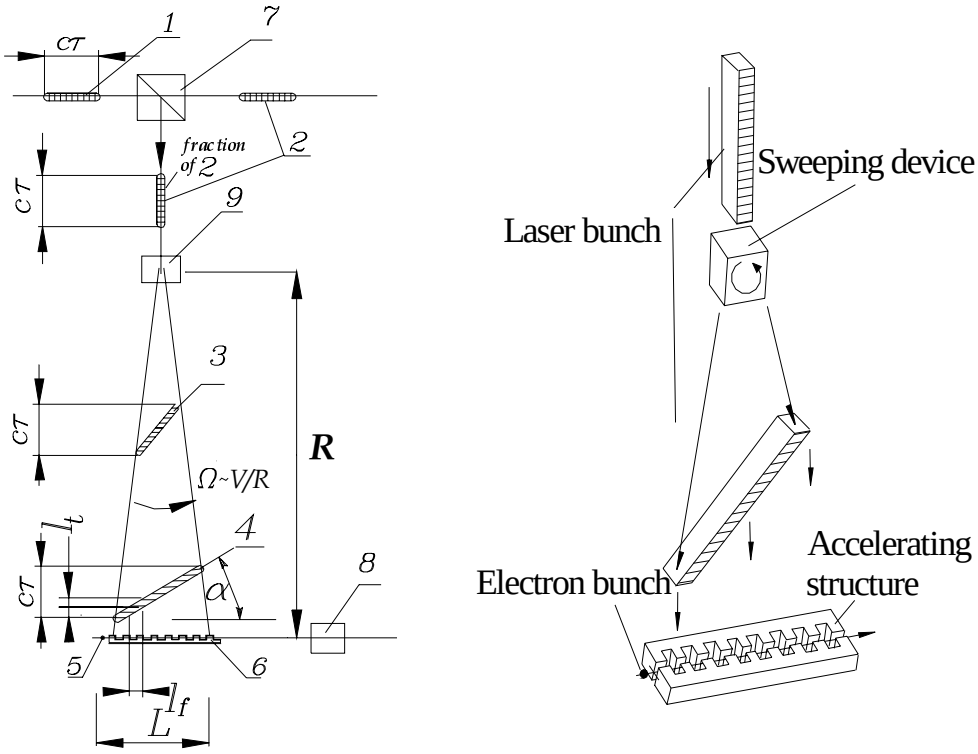

FIGURE 3: The TLF principle. At the right an isometric view is represented. The numbers 1, 2, 3 and 4 are numbering the laser bunch positions in four different moments of time. The length of the laser bunch is $c\tau$. This projection of the laser length to the radius vector always remains $c\tau$. 5 –is the particles' beam, what is going through the accelerating structure 6. 7–is a splitting device, 8–is a focusing element, 9–is a sweeping device. The lines across laser bunch show the wavefronts. This is a single accelerating module. l_f and l_t –are the cross-sections of the bunch in longitudinal and transverse directions respectively. Each point on the structure illuminated during the time $\approx l_t / c$.

The condition of synchronism is $\Theta \cdot \tan\alpha = \dfrac{cL}{VR}$, where $\Theta \cong L/R$.

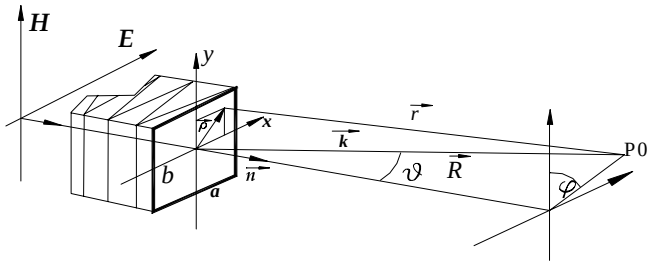

FIGURE 4: The system of coordinate in integration over output plane of the sweeping device.

For the focusing and deflecting the radiation at the same time, the phase variation across the aperture of the deflecting device must be as the following: $\chi(x,y) = \delta \cdot x + \kappa x^2$. The ordinary optical lens gives the necessary parabolic phase distribution. In this case the integral transforms into

$$H(t) = -\frac{ikH_0}{2\pi}\frac{\exp(ikR)ab}{2R}e^{i\omega t+\psi}\int_{-1}^{+1} e^{i(\alpha_1-\delta)\xi - i\kappa a^2\xi^2/4}d\xi .$$

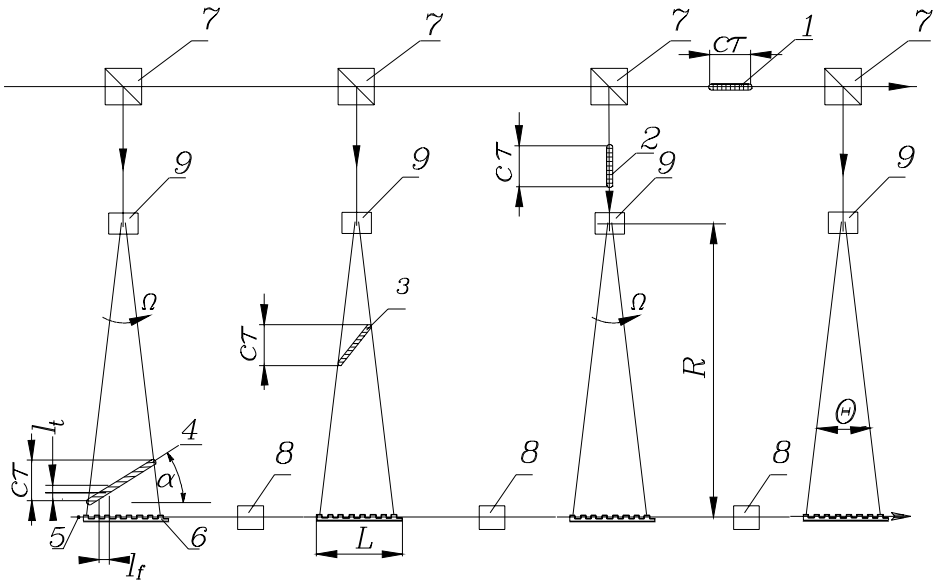

FIGURE 5: Accelerating complex scheme. 1–4–are the instant laser bunch positions; 1–is a primary laser bunch which is moving from the left side on the picture to the right. 5– is the beam of accelerated particles. 6–is the accelerating structure. 7–are the optical splitters. 8–are the particles' beam focusing elements (in additional to RF focusing). 9–are the sweeping devices. The distances between the structures are increased for better view.

So one can conclude that parameters of sweeping device are crucial for TLF method.

4. SWEEPING DEVICE

The device can be characterized by a deflection angle ϑ and the angle of natural diffraction $\vartheta_d \cong \lambda / a$, where a —is the aperture of the sweeping device.

The ratio of deflection angle to diffraction angle, is a fundamental measure of the quality for any deflecting device. This ratio defines the *number of resolved spots (pixels)* on the surface of the structure, $N_R = \vartheta / \vartheta_d$ **.**

The deflection angle could be increased by appropriate optics, but the number of resolved spots N_R is *an invariant* under such transformations.

N_R value gives the number for the lowering the laser power required for gradient desired and, also, the number for the duty time reduction. So it is desirable to have this number as big as possible.

Electro-optical devices use controllable dependence of refractive index on electrical field strength and direction applied to some crystals. The refractive index in active media has a dependence like

$$1/n_i^2 = 1/n_{0i}^2 + \sum_j r_{ij} \cdot E^j ,$$

where r_{ij} –are 6×3 tensor. Index *i* runs from 1 to 6. 1 stands for *xx*, 2–for *yy*, 3– *ss*, 4– for *ys*, 5–for *xs*, 6– for *xy*, *s*-longitudinal coordinate. Indicatrix allows to determinate the refraction index *n* components for monochromatic plane waves as a function of their polarization.

$$\Delta(1/n)_i = 1/n_i - 1/n_{0i}$$

$$\begin{pmatrix} \Delta(1/n^2)_1 \\ \Delta(1/n^2)_2 \\ \Delta(1/n^2)_3 \\ \Delta(1/n^2)_4 \\ \Delta(1/n^2)_5 \\ \Delta(1/n^2)_6 \end{pmatrix} = \begin{pmatrix} r_{11} & r_{12} & r_{13} \\ r_{21} & r_{22} & r_{23} \\ r_{31} & r_{32} & r_{33} \\ r_{41} & r_{42} & r_{43} \\ r_{51} & r_{52} & r_{53} \\ r_{61} & r_{62} & r_{63} \end{pmatrix} \times \begin{pmatrix} E_x \\ E_y \\ E_s \end{pmatrix},$$

where the vector $\vec{E} = \{E_x, E_y, E_s\}$ describes the electrical driving field applied.

The change of reflecting index is equal

$$\Delta n_i \cong (\partial n_i / \partial E_j) E^j(t) \cong -n_{0j}^3 r_{ij} E^j / 2$$

Typical values of the r_{ij} are of the order $\cong 10^{-12} m/V$. For example, for *GaAs (ZnSe, CdTe)* cubic structure and for *KDP (ADP, $CdGeAs_2$)* tetragonal structure we have correspondingly

$$(r)_{ij} = \begin{pmatrix} 0 & 0 & 0 \\ 0 & 0 & 0 \\ 0 & 0 & 0 \\ 1.5 & 0 & 0 \\ 0 & 1.5 & 0 \\ 0 & 0 & 1.5 \end{pmatrix} \times 10^{-12}[m/V], \qquad (r)_{ij} = \begin{pmatrix} 0 & 0 & 0 \\ 0 & 0 & 0 \\ 0 & 0 & 0 \\ 8.8 & 0 & 0 \\ 0 & 8.8 & 0 \\ 0 & 0 & 10.5 \end{pmatrix} \times 10^{-12}[m/V]$$

For a ***prism-based device*** deflecting angle defined by the phase delay across the laser beam front arising from differences in the path lengths in material of the prism having a refractive index *n*.

$$\vartheta \cong n \frac{(L_a - L_b)}{w}.$$

Here *w* –is the width of incident laser beam, L_a and L_b –are the distances through which the edges of the laser beam traverse the prism, Fig.6.

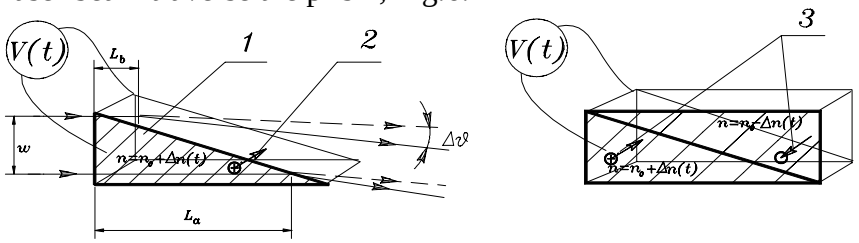

FIGURE 6: The prism deflection device concept. At the left side, the electro-optical crystal prism has metallization 1 (hatched) on both basements of the prism. Direction of optical axis had shown by 2. Time dependent voltage applied to metallization. At the right side *two* prisms have oppositely oriented optical axes 3 with the same polarity of electrical field applied.

A change in refractive index value yields a deflection angle change. To arrange such a change in refraction index, the basements of the prism are covered by metallization. When a voltage *V*(*t*) applied to the metallization, the refractive index changes $\Delta n = \Delta n(V(t))$, what yields the change in deflection angle as

$$\Delta\vartheta \cong \Delta n \frac{(L_a - L_b)}{w}.$$

For such a sweeping device, a lot of electro-optical crystals can be used, see Table 1 below. For example, a crystal *KDP* (KH_2PO_4) is transparent for a radiation with the wavelength $\lambda \cong 0.2 \div 1\,\mu m$. Some other crystals, such as a *CdTe, CuCl, GaAs, ZnTe, ZnS* are transparent in the region of wavelengths around $\lambda \approx 10\,\mu m$. The last group of materials have rather high refractive indexes n_0~(2-4) what compensate smaller electro- optical coefficient.

The number of resolvable sports for this device N_R can be found now as

$$N_R \cong \frac{\Delta\vartheta}{\lambda / a} = \frac{\Delta n \cdot (L_a - L_b) \cdot a}{\lambda w} \cong \Delta n \frac{l}{\lambda},$$

where $l = L_a - L_b$ stands for the prism base length and $a / w = 1$ in our case. Substitute for example the numbers for *ZnTe* (transparent for CO_2 laser radiation) which has $n_o \approx 2.9$, $r_{41} \cong 4.4 \cdot 10^{-12} m/V$, $E \cong 10 kV/cm \equiv 10^6 V/m$ one can obtain $\Delta n \cong 10^{-4}$.

For *KTN* (*Potassium Tantalate Niobat*) crystal $\Delta n \cong 7 \cdot 10^{-3}$ for $\lambda \cong 0.63 \mu m$ is possible. Anyway, the shorter wavelength is preferable from this point of view.

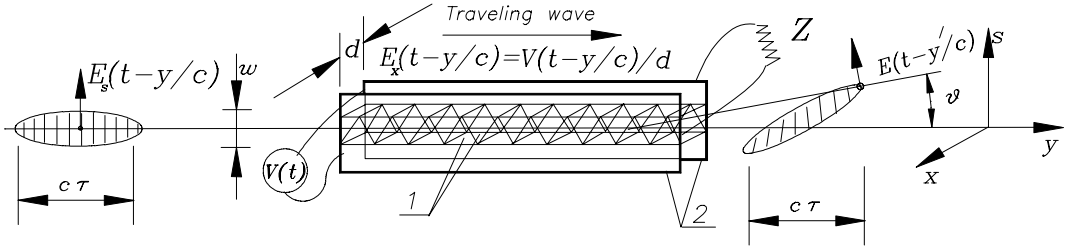

FIGURE 7: Prisms 1 with *oppositely directed optical axes* installed in series between two parallel strip–line electrodes 2, *d*–is the distance between them. *Z*– is matching impedance. Lines across the laser bunch schematically show the wave fronts. $E_x(t - y/c)$–is a driving electrical field.

The deflection angle and the number of resolved spots become now

$$|\Delta\vartheta| \cong \Delta n \frac{2L_d}{w} \cong \frac{L_d}{w \cdot d} n_0^3 \cdot r_{ij} \cdot V, \qquad N_R \cong \Delta n \frac{2L_d}{\lambda}$$

where L_d stands for full length of deflecting device, *w*–is the laser beam width (along direction of deflection). For *L*=50*cm*, one can expect for $w \cong 1cm$, that deflection angle is $\Delta\vartheta \cong 10^{-2}$ and $N_R \cong 10$ for $\lambda \cong 10\mu m$ and, correspondingly $\Delta\vartheta \cong 10^{-2}$ and $N_R \cong 100$ for $\lambda \cong 1\mu m$. We estimated the field applied to the crystals as 10 *kV/cm*.

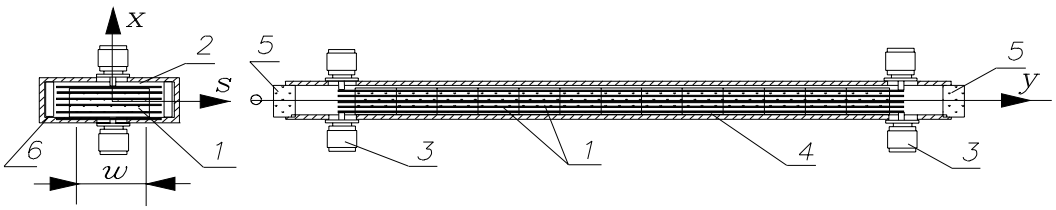

FIGURE 8: Example of technical realization of multi-prism traveling wave sweeping device. Electro-optical crystals 1 are positioned between strip-lines 2, attached at the end to the connectors 3. 4–is a cabinet with optical windows 5 from both sides. 6–is a matching dielectric.

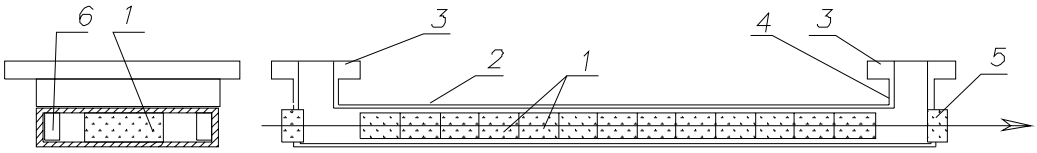

FIGURE 9: Multi-prism traveling wave sweeping device in a waveguide. 1–is electro-optical crystals, positioned in a waveguide 2, having bends 4 with flanges 3. 5–is an optical window. 6 –is a matching dielectric.

A lot of slowly operating devices is routinely in use.
Voltage applied about $V = \pm 5kV$ provided the deflection angle $\theta = \pm 10^{-3} rad$ in *KDP* device. The device has 10 *KDP* crystals with total 20c*m* length and about $1cm^2$ of input aperture.

TABLE . Electro-optical materials for deflector

Wavelength	Materials	ϑ , *rad*	N_R
$\lambda \cong 10\mu m$	*GaAs, ZnTe, ZnS, CdS, CdTe, CuCl*	0.01-0.02	10
$\lambda \cong 5\mu m$	*$LiNbO_3$, $LiTaO_3$, CuCl*	0.01-0.02	20
$\lambda \cong 1\mu m$	*KDP, DKDP, ADP, KDA, $LiNbO_3$*	0.01-0.02	100

Attenuation is 0.05%/*cm.*

Optimization.

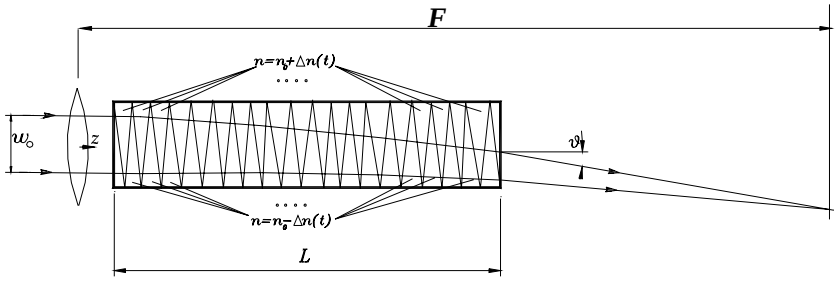

FIGURE 10: Dimensions used in optimization procedure.

$$L_{opt} \cong w_0 \cdot \sqrt{\frac{2}{3Kw_0}} \approx \frac{2}{3}F \, .$$

Mechanical deflection system

Angular frequency of sweeping required is equal $\Omega \cong V / R$, and the spot sweeped along the structure, so $\Theta \cong \Omega\tau \cong c\tau / R \cong L / R$, Estimating $R \cong 1m$, we obtain $\Omega \cong 3 \cdot 10^8$ *rad/sec* for *V* = *c*. The corresponding frequency $f_m \cong \Omega / 2\pi \approx 47\ MHz$.

So the frequency of mechanical oscillation of the mirrors must be $f_m / M \cong 5MHz$ in ten-stage tandem.

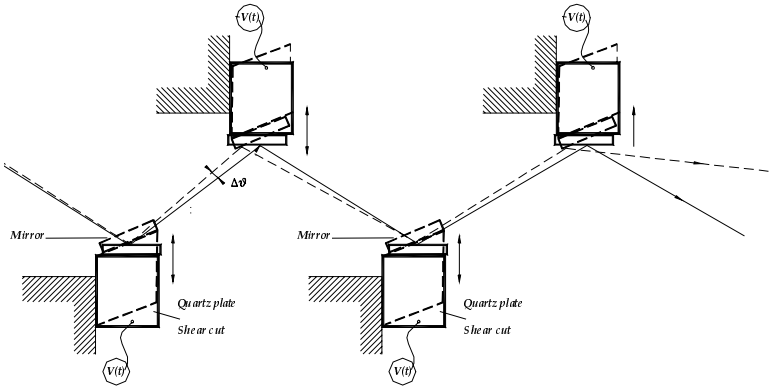

FIGURE 11: Deflection arrangements with quartz plate shear cut. This cut done with angle~55° to the Y- axis of the quartz crystal. Metallization applied to the front and opposite sides of the crystal. Tilt angle shown is not in scale (unfortunately).

For a *single* mirror attached to a piezoelectric, peak-to-peak angular motion with frequency around 5 *MHz* $\Delta\vartheta \cong 8.7 \cdot 10^{-4} rad$ is possible. Ten mirrors will give $\Delta\vartheta \cong 8.7 \cdot 10^{-3} rad$, what is acceptable. $N_{\max} \cong \dfrac{\sqrt{\Delta\vartheta}}{\lambda_{ac} / w} \cong \dfrac{1}{10^{-3}} \cdot \sqrt{8.7 \cdot 10^{-4}} \cong 30$ for $\lambda_{ac} \cong 10\mu m$ and $w \cong 1cm$.

For $\lambda_{ac} \cong 1\mu m$, the number of resolved spots will achieve $N_{\max} \cong 300$.

So this is probably mostly effective sweeping device. It definitely could be used at the proof of principle stage.

Acousto-optical deflector

$$\Delta\vartheta \cong \frac{\lambda}{v}\Delta f \cong \frac{\lambda}{w}\tau \cdot \Delta f \ ,$$

where we recalled the time required for the wave to pass trough the laser beam width w as $\tau = w / v$ and Δf stands for the range of frequency change.

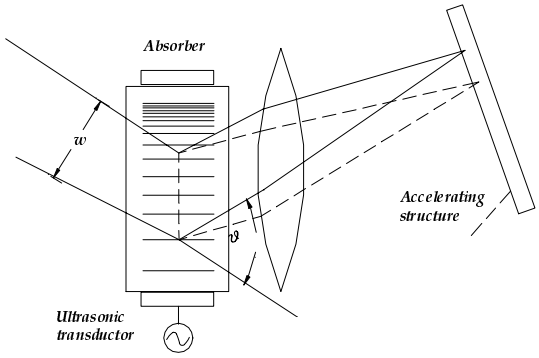

FIGURE 12: Acousto-optical deflection.

The number of resolved sports

$$N_R \cong \frac{\Delta\vartheta}{\lambda / w} \cong \tau \cdot \Delta f \ ,$$

so the product of bandwidth and crossing time is crucial for this method.
For example, for typical velocity $v \cong 0.6mm/\mu s$, $w \cong 5mm$ the time will be about $\tau \cong w / v = 5 / 0.6 \cong 8\mu s$. To obtain a reasonable number $N_R \approx 20$, one needs to have $\Delta f \cong N_R / \tau \cong 20 / 8 = 2.4MHz$.

Short laser bunch.

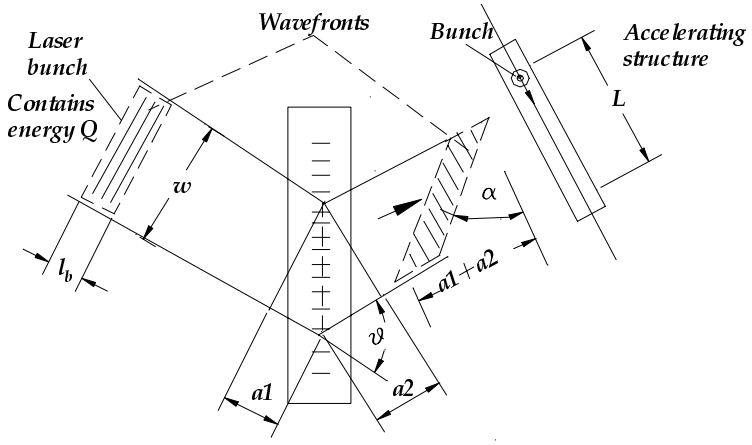

FIGURE 13: A short laser bunch diffraction with arrangements from previouse Figure.

Distribution of diffracted radiation among the other maximums is another difficulty with the grating.

General conclusion is that the laser beam deflectors are available with parameters necessary for successful sweeping.

5. ACCELERATING STRUCTURE

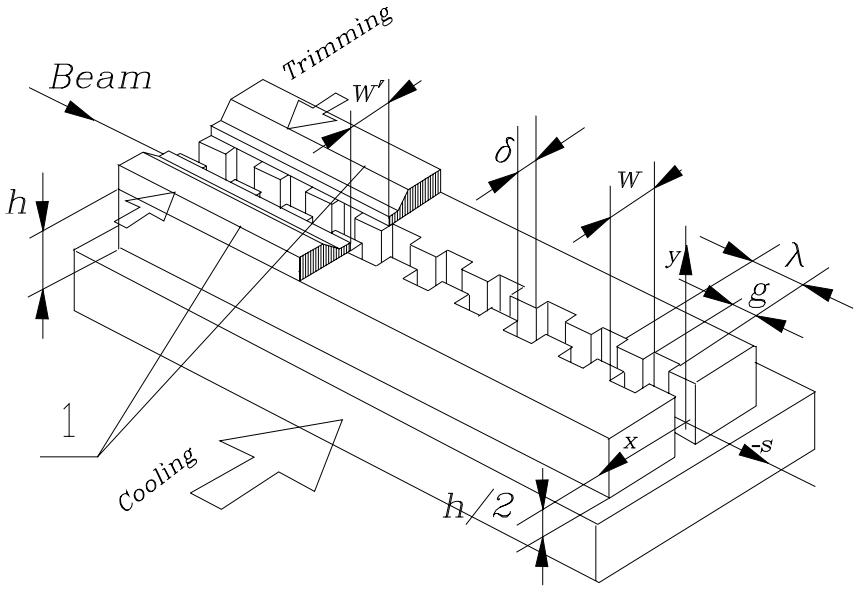

FIGURE 14: The foxhole type accelerating structure. Height h is $h \cong \lambda_W / 2$, where λ_W –is a wavelength of laser radiation inside the cell. $g / \lambda \cong 1/2$, $W \cong 0.7\lambda$, $\delta \cong 0.2\lambda$. 1–are the masks along the structure. $W' \le W$. The masks are used for trimming the inductive coupling (Q_{RF}-factor).

This structure has advantages in pumping, alignment and cooling.
It is mechanically strong and could be easily fabricated with nanolithography.
Good 3D positioning for electrical field map.
The height $h \cong \lambda_W / 2$.
Exact dimensions define the balance between the power going in the cell and back. Higher value of Q_{RF} reduces the power required from laser to reach the gradient desirable. But *mostly*

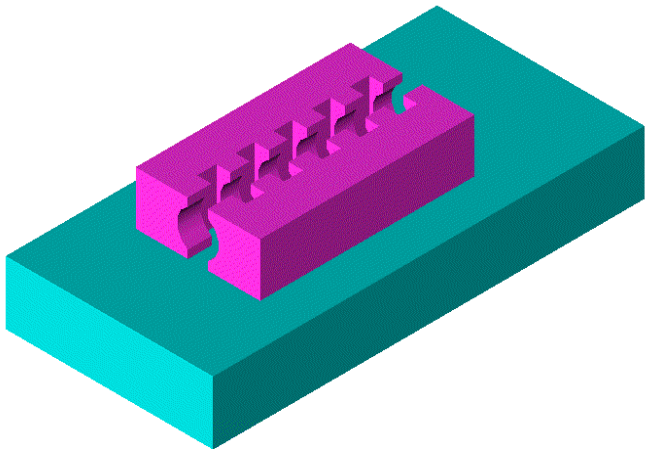

FIGURE 15: An example of the structure with round passing holes. Dimensions are the same as on Fig.4.1. Covers (masks) are not shown. Five cells are shown.

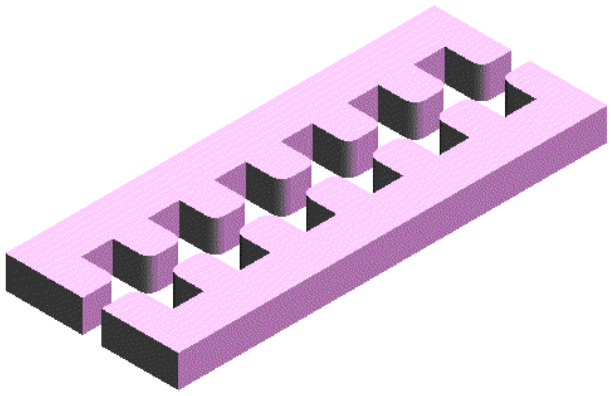

FIGURE 16: An example of the structure with smoothed passing holes. Covers and base are not shown. For better visibility the height shown is reduced also.

Typical longitudinal and transverse wakes *normalized to one cell* are $W_{\parallel} \cong -7\,kV/pC$ and $W_{\perp} \cong 2.2 \cdot 10^2 V/pC/\mu m$ correspondingly for the accelerating structure with $\lambda \cong 10\mu m$, $\delta = 2\mu m$, $W = 7\mu m$ and the bunch with the longitudinal length $\sigma_l \cong 1\,\mu m$ and bunch population $N \cong 10^6$.
Total charge is $eN \cong 1.6 \cdot 10^{-13} C$ or $0.16pC$.

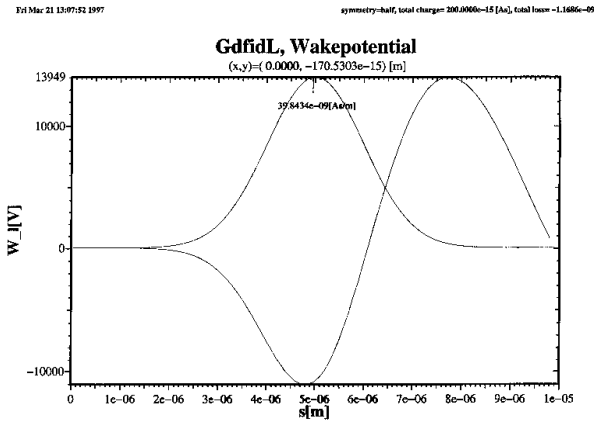

FIGURE 17: Example of the wake for 5 cells. Wake in the center of the bunch is about -10 *kV*. Charge in the bunch is ~0.2 *pC*.

So one can see compare the wake energy drop $\approx 7kV/pC \times 0.16\,pC \cong 1.12kV$ with the energy gain in one cell as ~30 *kV*. So the accelerating voltage drop is about ~1.12/30 ≅ 3.7%. The energy, carried out of the cell is, hence ~7.4%.

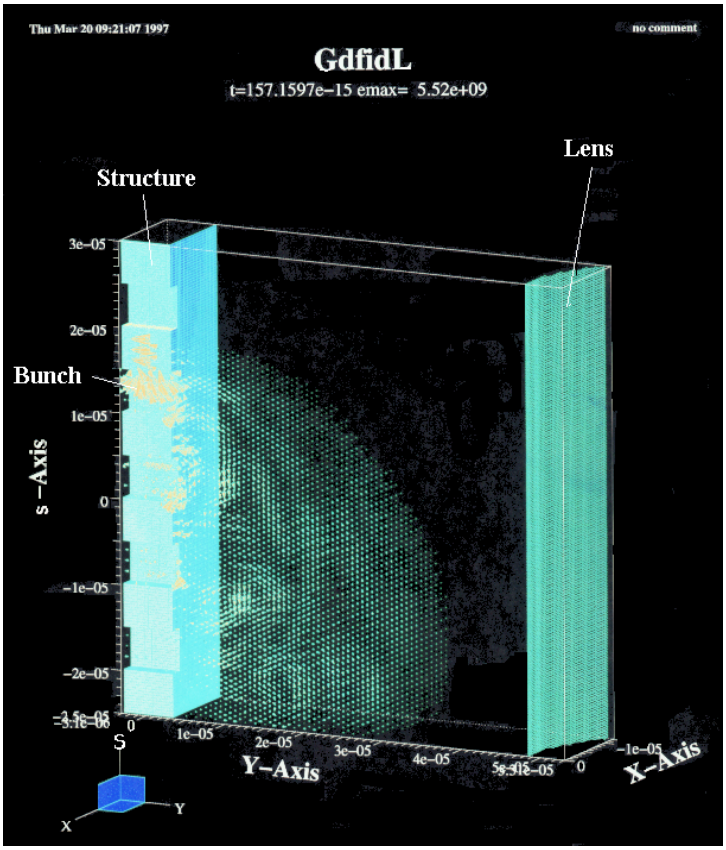

FIGURE 18: The bunch in the structure. A half of full picture is represented. The bunch is running through the structure on the left. A cylindrical lens; ¼ of the geometry is shown.

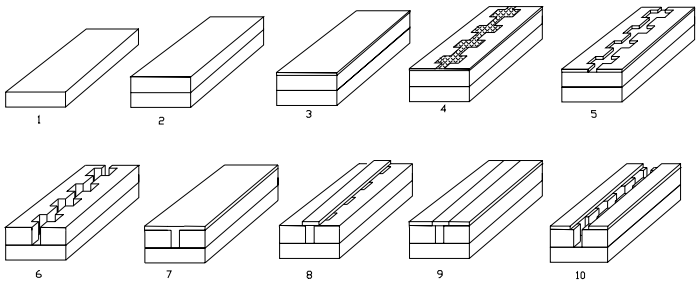

FIGURE 19: Fabrication of the structure. 1– is a base. 2–material of the structure is placed on the base. 3–a photoresist is placed at the top. 4–the photoresist is exposed. 5–some of photoresist is removed. 6–material of the structure etched. 7–a new cover of photoresist is placed. 8–extra resist is removed. 9–material of the structure is added. 10–structure etched again.

General conclusion is that there is a structure, acceptable for particle acceleration with wavelengths $\lambda_{ac} \cong 1-10\mu m$**.**

6. SOME TECHNICAL DETAILS OF THE SCHEME

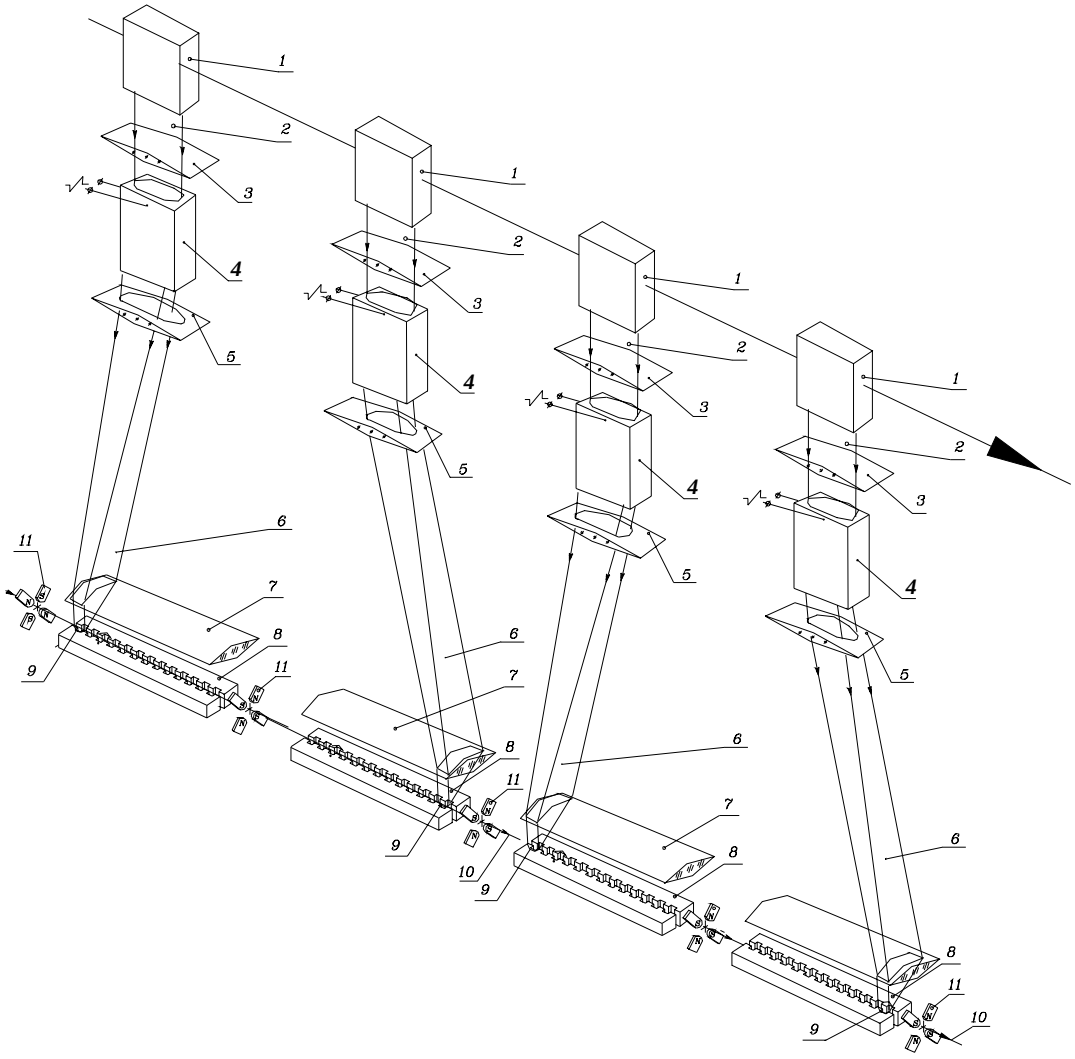

FIGURE 20: The Accelerating assembly. This is an isometric view from Fig.5. Some elements were added. 1–are the splitting devices. 2–is the laser bunch envelope. 3 and 5–are the lenses for longitudinal focusing. 4–is the sweeping devices. 6–is the instant directions of the laser bunch deflected. 7–is a cylindrical lens for transverse focusing of the laser beam. 8–are the accelerating structures. 9–is the focused laser spot. 10–is the electron beam trajectory. 11–are the focusing quadrupoles.

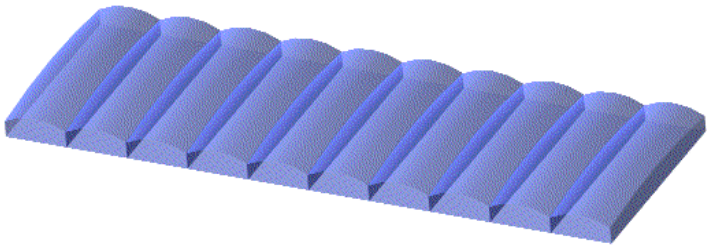

FIGURE 21: An isometric view of short focusing cylindrical lens, 7. Each of the pieces focuses the incoming laser radiation to individual opening of the structure. Basically the surface of each element of this lens is a part of sphere. Picture is not in scale. Period equals to the period of the structure, what is the wavelength of the laser radiation. This also could be treated as diffraction pattern.

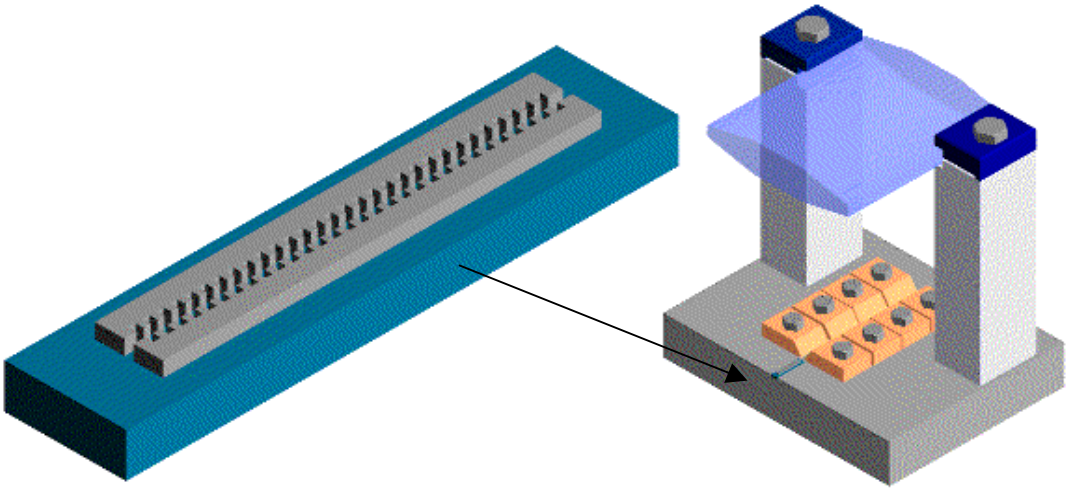

FIGURE 22: An isometric view of accelerating structure and cylindrical lens. Structure on the left is scaled. Covers on accelerating structure are not shown. The short focusing lens is shown simplified also.

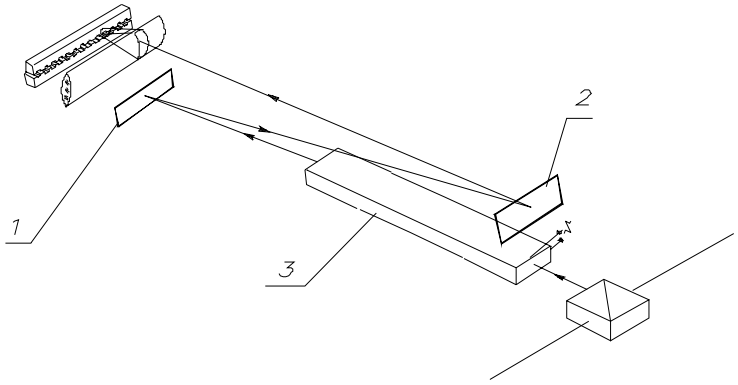

FIGURE 23: The way to increase the distance between deflecting device and accelerating structure. 1,2 –are the mirrors, 3–is the deflecting device. Mirrors might be slightly curved to obtain some focusing properties.

.

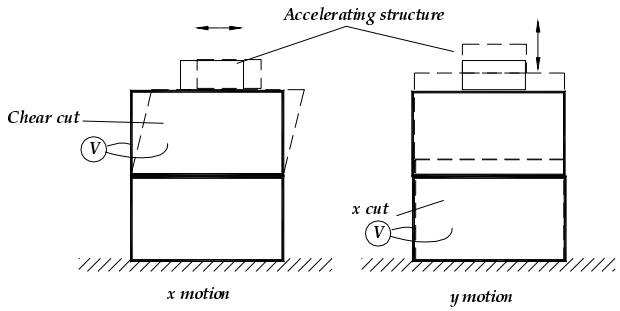

FIGURE 24: The concept of transverse movers for accelerating structure. Two piezoelectric plates have different types of cuts with respect to the crystallographic axes.

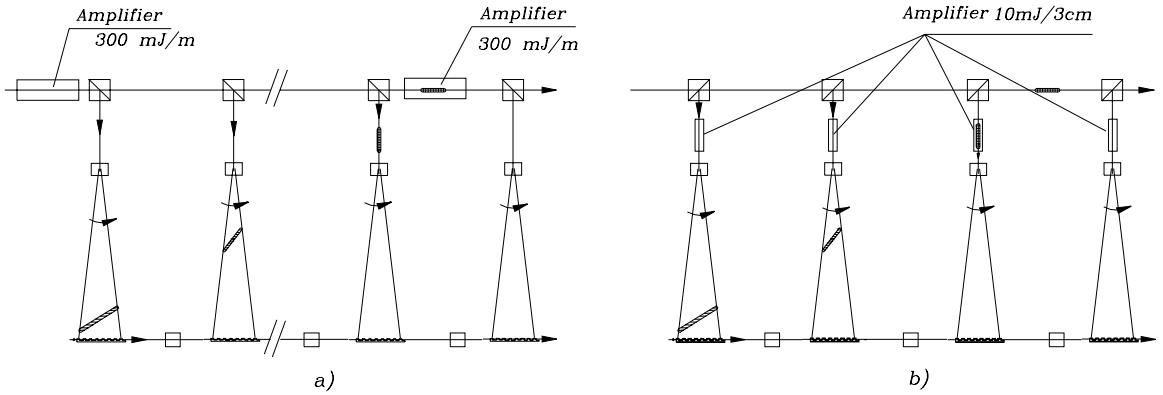

FIGURE 25: Possible installations of amplifiers. a) –Sectioning with few structures. b) –Each 3*cm* section has it's own amplifier.

Each part of the grating structure is illuminated by duration, which is defined by longitudinal size l_t. For example, if we consider $l_t \cong 100\lambda$, $\lambda = 1\mu m$, then $l_t / c \cong 3 \cdot 10^{-13} sec$. For $\lambda = 10\,\mu m$ this value is ten times more. This time is less than the time between electron-electron collisions $\tau \approx l_{free} / v_F \cong 10^{-12} sec$, where l_{free} is the free path length, v_F is the electron velocity at Fermi surface. The time of illumination still, however longer, than the time, corresponding to reaction of electron plasma in metal $\tau \cong 2\pi / \omega_p = 2\pi / \sqrt{4\pi n r_0 c^2} \approx 3 \cdot 10^{-16} sec$, where n is the electron density in a metal.

7. INJECTION SOURCE

It was shown for the first time by author, that there exists a strong quantum limitation for the lowest emittances in the bunch like

$$(\gamma\varepsilon_x)(\gamma\varepsilon_y)(\gamma\varepsilon_s) = (\gamma\varepsilon_x)(\gamma\varepsilon_y)(\gamma l_b(\Delta p / p_0)) \geq \tfrac{1}{2}(2\pi\lambda\!\!\!^{-}_C)^3 N\,,$$

where $\lambda\!\!\!^{-}_C = r_0/\alpha$ –is a Compton wavelength, $r_0 = e^2/mc^2$–is a classical electron radius, $\alpha = e^2/\hbar c$–is a fine structure constant, $\gamma = E/mc^2$, N–is a bunch population, l_b–is a bunch length, $\Delta p / p_0$–is a relative momentum spread in the bunch, $(\gamma\varepsilon_s) = \gamma l_b(\Delta p / p_0)$–is an invariant longitudinal emittance.

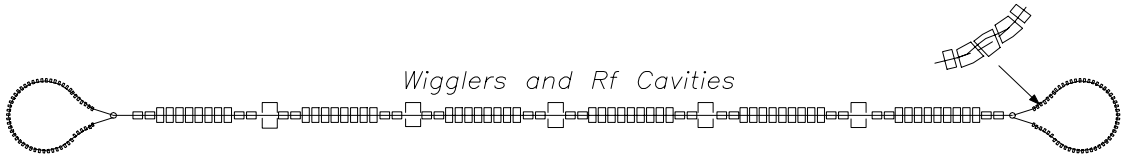

FIGURE 26: A Kayak-paddle cooler. The length of straight section might be a few hundred meters. Bends made with many short period divisions to prevent emittance dilution. In first approximation it could be considered as a *very* short-period *planar* wiggler with lot of bending elements. Each element of this bend could be considered as an achromatic three-magnet bend with the focusing quads in between. One of the three-magnet bending elements is represented in scale at the right top. It has three magnets and two quads.

In this cooler a particle needs to re-radiate its full energy few times, like in ordinary damping ring. The rate of energy losses is given by

$$d\gamma / ds \cong -\frac{2}{3} r_0 \frac{K^2}{\lambda\!\!\!^{-2}} \gamma^2 ,$$

For so called characteristic-damping length one can obtain

$$l_s = -\frac{\gamma}{d\gamma / ds} = \frac{3}{2} \frac{\lambda\!\!\!^{-2}}{r_0 K^2 \gamma} .$$

One can see that $1/l_s$ has *linear* dependence on energy. For parameters under discussion

$$l_s = -\frac{\gamma}{d\gamma / ds} \cong \frac{2 \cdot 10^3}{7.5 \cdot 10^{-4}} \cong 2.6 \cdot 10^6 m .$$

The cooling time associated with this length is $\tau_{cool} \cong l_s / c$.

One can see from here, that the cooling (damping) time *does not depend on the wiggler period*.

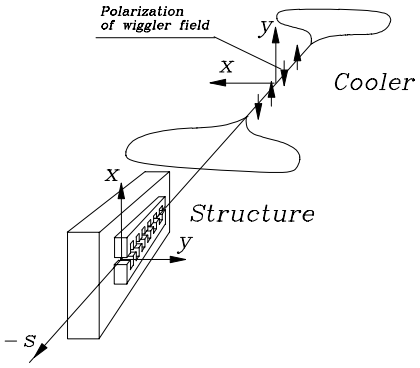

FIGURE 27: Relation between coordinates of the cooler and the structure. Polarization of the wiggler field is vertical; the bends of cooler are going in horizontal plane. If polarization of the wiggler field is horizontal, the x coordinates might be the same, and the cooler plane and the plane of the structure may coincide.

Equilibrium emittances

$$(\gamma\varepsilon_x) \cong \tfrac{1}{2} \cdot \lambda\!\!\!^{-}_C \overline{\beta}_x (1 + K_x^2 / 2) \gamma / \rho_x \cong \tfrac{1}{2} \cdot \lambda\!\!\!^{-}_C \overline{\beta}_x (1 + K_x^2 / 2) K_x / \lambda\!\!\!^{-}$$

$$(\gamma\varepsilon_y) \cong \tfrac{1}{2} \cdot \lambda\!\!\!^{-}_C \overline{\beta}_y \gamma / \rho_x \cong \tfrac{1}{2} \cdot \lambda\!\!\!^{-}_C \overline{\beta}_y K_x / \lambda\!\!\!^{-} ,$$

where $\overline{\beta}_{x,y}$ – are averaged envelope functions in the wiggler. The last formulas together with $\tau_{cool} \cong \frac{3}{2} \cdot (\lambda\!\!\!^{-2} / r_0 c K^2 \gamma)$, define the cooling dynamics under SR.

One can see that equilibrium invariant emittances *do not depend on energy*. In addition, quantum equilibrium *vertical emittance* and the cooling time do not depend on the wiggler period at all. Ratio $(\gamma\varepsilon_x) / (\gamma\varepsilon_y) \cong (1 + K_x^2 / 2) \overline{\beta}_x / \overline{\beta}_y$.

Substitute for estimation $\overline{\beta}_{x,y} \approx 1m,\ \lambda\!\!\!^{-} \cong 5cm, K \cong 5$, one can obtain for *quantum emittances* the following estimations

$$(\gamma\varepsilon_x) \cong 2.5 \cdot 10^{-8}\ cm \cdot rad , \quad (\gamma\varepsilon_y) \cong 9.5 \cdot 10^{-10} cm \cdot rad .$$

KPC satisfies has $\eta \cong -0.0001$.

Diluted bunch.

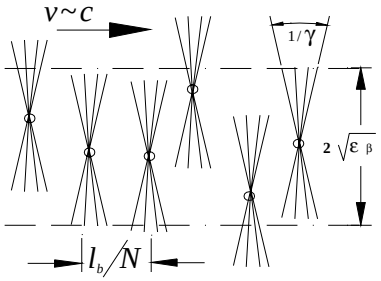

FIGURE 28: Diluted bunch.

So one can see, that even for such tiny emittances (dimensions) the space charge effects does not look as drastic ones.

Solid-state source of low emittance electron and ion beams.

Typical divergence from tip is about 1/100 *rad*. Now it is possible to obtain the tips with nanometer-level radius routinely. So the emittance of the electron beam, one could expect here be

$$\gamma\varepsilon \cong 10^{-7}\, cm \cdot 10^{-2}\, rad = 10^{-9}\, cm \cdot rad\ .$$

This is an invariant emittance, as the electrons are nonrelativistic.
The tips described above routinely working with currents ~100 *nA*. The last number gives the total charge ~10^{-7} *Q/s*. In its turn, this corresponds to $N \cong Q/e \cong 6.25 \cdot 10^{11}$ electrons per second. The longitudinal emittance defined by the temperature of the tip. In any case the longitudinal energy spread is less, than the work function eU_W.

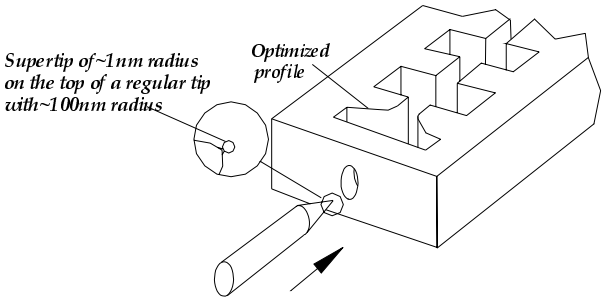

FIGURE 29: Schematic view of a tip installed on the holder. All elements illuminated by the same laser source swept. Tip is not shown in scale and shown removed from the cell.

For estimation $\beta_x \approx l_b \approx 1 cm$, $N \approx 10^6$, $\gamma \cong 1$, one can obtain $\gamma\varepsilon_x \le 0.87 \cdot 10^{-7}$ *cm rad*. This is estimation for the *maximal* possible transverse emittance required for degeneration of the bunch with population indicated. So one can conclude, that here we are close to manifestation of quantum effects.

Ion source is pretty much the same

Bunching

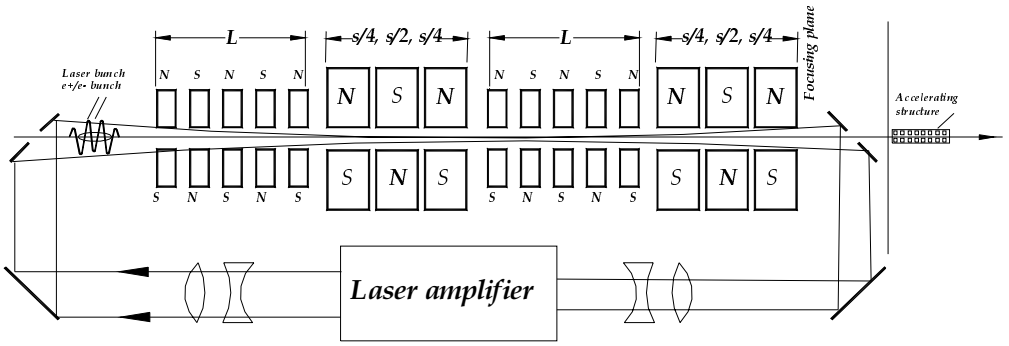

FIGURE 30: Cascade bunching scheme. *K* factor in second wiggler is other, than in the first one. This scheme is an analog of a Klystron with two cavities and two drifts

The minimal energy defined by the limitation due to the space charge effects, characterized by the plasma frequency

$$\omega_p^2 \cong \frac{4\pi n r_0 c^2}{\gamma^3},$$

which yields $E = mc^2\gamma \approx 4.5 MeV$ the total energy.

7. TRANSVERSE FOCUSING DURING ACCELERATION

Quadrupole lenses

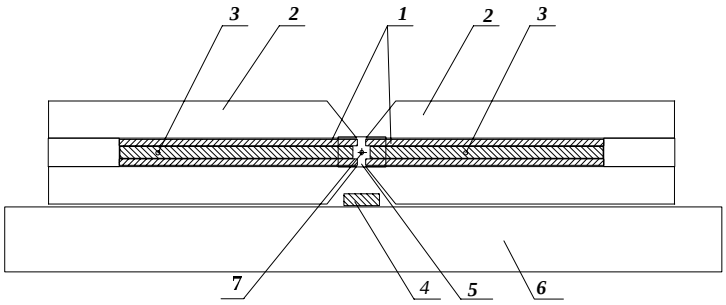

FIGURE 31: Example of a quadrupole design. Transverse cross-section is shown. Longitudinal dimension (perpendicular to the plane of drawing) is about 0.5 *cm*. Accelerating bunch is moving perpendicular to the plane of the drawing. 1–is an iron blades-like looking poles, 2–is a yoke, 3–is a current strips, 4–is a current strip for vertical axes trim, 5–is a profile of the accelerating structure, 6–is a base, 7–is a cross-section of the accelerating bunch.

RF focusing

Resulting transverse force could be expressed as

$$\frac{dp_\perp}{ds} \cong -\frac{er}{2\lambda_{ac}}\{\lambda_{ac}[\frac{\partial E_s}{\partial s}+\frac{1}{v}\frac{\partial E_s}{\partial t}]+\frac{2\pi c}{\gamma^2 v_p}\frac{\partial E_s}{\partial \varphi}\}$$

$$\langle F_x\rangle \cong \frac{e\lambda E_m}{W^2} Sin\varphi \cdot x, \quad \langle F_y\rangle \cong \frac{e\lambda E_m}{h^2} Sin\varphi \cdot y, \quad \langle F_s\rangle \cong \frac{2eE_m}{\pi} Cos\varphi .$$

These forces are quadrupole types for the particles out of the crest of RF. The effective focusing factor of the RF lens can be evaluated as

$$k_x = -\frac{1}{pc}\frac{\partial\langle F_x\rangle}{\partial x} \cong -\frac{e\lambda_{ac}E_m}{mc^2\gamma W^2}Sin\varphi\,, \quad k_y = -\frac{1}{pc}\frac{\partial\langle F_y\rangle}{\partial y} \cong -\frac{e\lambda_{ac}E_m}{mc^2\gamma h^2}Sin\varphi\,.$$

Substitute here $\lambda_{ac} = 10\mu m$, $\gamma = 2\cdot 10^4$ (pc=10 GeV), $W \approx 5\mu m$ (see Fig.4.1), $E_m \approx 10^{11} V/m$, we obtain $k_x \approx 4\cdot 10^5 \cdot Sin\varphi[m^{-2}]$.

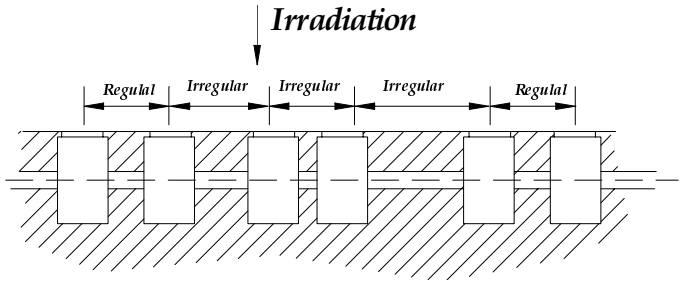

FIGURE 32: Arrangement of the phase shifts in the cells.

Anyway one can see that the RF focusing could be, in principle, two orders of magnitude more strong, than one uses a conventional quad, scaled to appropriate level.
Simplest Foxhole structure focuses the beam in direction across the narrowest size of passing holes, *x*.

9. ACCELERATING GRADIENT

$$E_m \cong 2\sqrt{Q/(\varepsilon_0 c\tau\lambda g)}$$

For estimation let us take $Q = 0.01J$, $\tau \cong 0.1\ ns$, $\lambda \cong 1\mu m$, $g \cong \lambda/2 = 0.5\mu m$.

This gives the field strength $E_m \cong 275 GeV/m$.

This value must be reduced by the factor, taking into account the longitudinal length l_f instead of *g*. The longitudinal length could be estimated as a $l_f \approx L/N_R$, where *L* –is the length of the structure, N_R –is the number of resolved spots.

For $\lambda \cong 1\mu m$ one can expect $N_R \approx 100$, so the length of our interest is $l_f \approx c\tau/N_R$, what is $l_f \approx 0.03cm \approx 300\lambda$.

So $E_m \cdot \sqrt{g/l_f} \approx 11.2 GeV/m$.

The value of electrical field *inside* the structure could be found by taking into account RF quality factor Q_{RF}, see section about accelerating structure. For $Q_{RF} \approx 9$ it could reach again $E_m\sqrt{Q_{RF}}\sqrt{g/l_f} \approx 33 GeV/m$ in conservative estimation. So despite of the radiation illuminates the orifice during $\sim l_f/\lambda_{ac} \approx c\tau/N_R/\lambda_{ac} \sim$ 300 periods we suggest such low Q_{RF}. This gives guaranties that equilibrium in cell established well.

So the laser flash with $Q \cong 10\,mJ$ at $\lambda \cong 1\,\mu\,m$ is able to feed the accelerating structure with the length about $c\tau \approx 3cm$ with ≥ 33 *GeV/m*. A flash with $Q \approx 1J$ will feed the 3-m total accelerating length, providing the energy gain $\approx 100GeV$. A pulse with $Q \approx 100\,J$ could feed 10 *TeV* machine and so on.
Density of energy falling on this area as high as $Q/S \cong Q/WL \approx Q/\lambda L \approx 3J/cm^2$ for $\lambda \cong 10\mu\ m$ and $30J/cm^2$ for $\lambda \cong 1\mu\ m$.

The illumination lasts for a time $t \cong l_t / c \cong l_f / c \cong 10^{-13}\,s$. Remind again, that this time is less than the time between electron-electron collisions, what is $\tau_{coll} \cong 10^{-12}\,s$, still however longer, than the time, corresponding to reaction of electron plasma in a metal, what is $\tau_p \approx 3 \cdot 10^{-16}\,s$.

Types of lasers for utilization in TLF method
TLF method promises up to 30 *TeV/km* or 300 *TeV* on 10 *km* with 0.3 *J/m* or with 3 *kJ* per pulse total for the 10 *km*. For lower energy the laser power is proportionally lower.
As it was mentioned the laser amplifier **could be sectioned**, Fig.25. So for 1 *km*, the total output power of the laser must be within 0.5 *MW* with repetition rate about 160 *Hz* for $\lambda_{ac} \cong 1\mu m$.
Nd-Glass lasers can be used here. For pumping the driving lasers the *diode laser arrays* could be used for the wavelengths indicated. This brings efficiency of the laser up to 10% level. This type of laser is probably the mostly powerful.
CO_2 laser based system gives lower final energy, but the total power required for 1 *km* is $P_i \cong Q/\tau \approx 3 \cdot 10^{12} W$. within routinely obtained. With 10*m* sectioning the power required from one stage of the laser amplifier goes to $P_i \cong Q/\tau \approx 3 \cdot 10^{10} W$ with total energy 3*J*. In *visible light the Nd:YAG* lasers working at doubled frequency are the best for application. The accelerating structure engineering and low emittance source adequate to this wavelength come to the edge of the present day technological possibilities however.
Lasers for the TLF method need to operate in intermediate time duration $\tau \approx 100ps$. *Equivalent time of illumination of any point on accelerating structure with TLF still however, very short –* $0.1 \div 1ps$ *only for* $\lambda_{ac} \cong 1 \div 10\mu m$ *respectively.*
We would like to stress here, that the TLF method allows reaching the field limit with the lowest energy of laser source. TLF method allows a drastic reduction of illuminating time also.

10. BUNCH POPULATION

The energy, accepted from the field by *N* particles is $W_a \cong eNE_m gI(g)$ where *e* is the charge of a particle, $I(g)$ is a function of the order of unity –an analog of the transit time factor. The share of the energy will be

$$\eta W \cong \eta \frac{Q\lambda}{2c\tau} \cong eNgI(g)\sqrt{\frac{Q}{\varepsilon_0 c\tau\lambda g}}\ .$$

Last relation emerges

$$N \cong \frac{\eta}{2eI(g)}\sqrt{\frac{\varepsilon_0 \lambda^3 Q}{c\tau\, g}}\,.$$

With $I(g)$= 0.5, $\eta \approx 0.05$ (i.e. only 5% of the energy stored in one cell carried out by the bunch), this yields $N \cong 1\cdot 10^6$ for $\lambda_{ac} \cong 1\mu m$. For $\lambda_{ac} \cong 10\mu m$ this number will be $N \cong 3\cdot 10^7$. One can compare the value $\eta \cong 5\%$ with what obtained from numerical calculations of wake fields (7.5% for one particular structure, Section 5). This means that our simple estimation is good enough.

Optimal length of the bunch.

$$\sigma_{b0}^3 \approx \frac{eNZ_0 c\lambda^2}{(2\pi)^{3/2} 4\pi^2 V_0} \ln\left(\frac{2g}{\delta}\right).$$

Substitute here $N \cong 10^7$, $g \cong 5\mu m$, $\delta \cong \sigma_b \cong 0.2\mu m$, $\lambda \equiv 10\mu m$, V_0~ 30 *kV* we obtain $\sigma_{b0}^3 \approx 23.5\cdot 10^{-12} cm$, and $\sigma_{b0} \approx 2.86\mu m$.

11. FINAL FOCUS

β^* in the interaction point must be of the bunch length value, what is about $0.1 \div 1\lambda_{ac}$, i.e. $\sigma_l \approx \beta^* \cong 0.5\mu m$. The envelope function value at the distance *s* from the interaction point will be, hence as big as

$$\beta \cong \beta^* + \frac{s^2}{\beta^*} \cong \frac{s^2}{\beta^*},$$

where we neglected the focusing, arising from the incoming bunch.
However

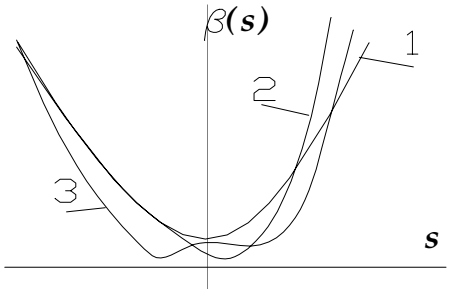

FIGURE 33: The envelope function behavior. 1 – corresponds to $K_F \cong 0$ or weak incoming bunch, 2 – corresponds to the same initial conditions as 1 but K_F is big, 3 –corresponds to the changed initial conditions, so the crossover shifted to the left. All envelope functions shown for the bunch moving from the left to the right.

Shift of focal point due to radiation, what is basically the same as the *lengthening* of the bunch

$$\Delta F \approx -\tfrac{3}{2}\cdot r_0 \gamma^2 \frac{(\gamma\varepsilon)}{\beta^*}\,.$$

We suggested an arrangement of the final focusing for our purposes as *a multiplet* of FODO structures. The number of the lenses in such a multiplet is around a few hundreds. This is so called ***Adiabatic Final Focus***. The gradient in these lenses must vary from the very strong at the side closest to IP, to a weak one at opposite side. Focusing properties of the RF lens, discussed above can be used here. A laser radiation of general and multiple frequency can be used for such focusing.

The laser radiation, phased with the main driving one can excite the single groove directly from the side. The quadrupole parameter described earlier. Substitute here $\lambda = 10\mu m$, $\gamma = 2 \cdot 10^6$ (pc=1TeV), $w \approx 5\mu m$, $E_m \approx 10^{11} V/m$, we obtain $k_x \approx 4 \cdot 10^4 \cdot Sin\varphi\,[m^{-2}]$. For $\varphi = \pi/2$ this expression has a maximum, this means, that the lenses are phased for the focusing only. The variation of the focusing strength has a quadratic dependence with the deviation ψ from the angle $\varphi = \pi/2$, $k_x \approx Cos\psi$. For the longitudinal length of the grove about $g \cong 5\mu m$, the focal distance will be

$$F \cong 1/kg \cong 1/4 \cdot 10^4 5 \cdot 10^{-6} = 5 \text{ [}Meters/cell\text{]}.$$

Equivalent gradient of the quadrupole lens is $G \cong 0.3pk \cong 1.2 \cdot 10^7 kGs/cm$. So the lens with ≈ 500 cells having the length $L_F \cong 0.5cm$ reaches the focal length $F \approx 1\ cm$.

Such a tiny lens, not sensitive to detector magnetic field can be easily installed inside the detector very close to the Interaction Point.

12. LUMINOSITY

$$L \cong \frac{N^2 f H_B \gamma \cdot N_B}{4\sqrt{(\gamma\varepsilon_x)(\gamma\varepsilon_y) \cdot \beta_x \beta_y}},$$

where H_B – is the enhancement parameter. N_B –is the number of bunches per train. For emittances $\gamma\varepsilon_x \cong 2.5 \cdot 10^{-8} cm \cdot rad$, $\gamma\varepsilon_x \cong 9.5 \cdot 10^{-10} cm \cdot rad$ and for $\beta_x \approx \beta_y \approx 0.3\lambda_{ac}$, $\lambda_{ac} \cong 10\mu m$, $\gamma = 6 \cdot 10^6$ (pc=3TeV), $N \cong 10^7$, $f \cong 160Hz$, H_B=1, N_B=1,

$$L \approx 1.7 \cdot 10^{34} cm^{-2} s^{-1}.$$

For $\lambda_{ac} \cong 1\mu m$ result will be about the same as the number of the particles is lower here. The transverse Gaussian size will be

$$\sigma_x \cong \sqrt{(\gamma\varepsilon_x)\beta_x^*/\pi\gamma} \cong \sqrt{2.5 \cdot 10^{-8} \cdot 3 \cdot 10^{-4}/2 \cdot 10^6/\pi} \cong 1.1 \cdot 10^{-9} cm\ (\equiv 0.11 \overset{o}{A})$$

$$\sigma_y \cong \sqrt{(\gamma\varepsilon_y)\beta^*/\pi\gamma} \cong \sqrt{9.5 \cdot 10^{-10} \cdot 3 \cdot 10^{-4}/2 \cdot 10^6/\pi} \cong 2.2 \cdot 10^{-10} cm\ (\equiv 0.022 \overset{o}{A}).$$

A small *crossing angle* required for prevention of irradiation of the final lenses by used beams. This angle is absolutely necessary for multi- bunch operational mode. Tiny dimensions of the beam can help to push the beams through.

Notice here that total length for acceleration up to 300 *GeV* could be about twenty meters, taking into account that a fraction of the accelerating sections is of the order 50%. As the total

energy of the full energy accelerator will be around *1 J*, what gives the average power of the order 160 *W*.
The beams of electrons and positrons could be polarized what gives the effective gain in luminosity and reduces the background.
The possibility of operation with high repetition rate, up to *few kHz* is favorable.

13. INTERACTION POINT

$$Y_0 \equiv \frac{2}{3}\frac{\hbar\omega_c}{E} = \gamma\frac{H}{H_c},$$

where H is the magnetic field, $H_c = m^2c^3/e\hbar \cong 4.4\cdot 10^{13}\ G$ is the Schwinger critical field strength, ω_c is the critical frequency of classical synchrotron radiation. This parameter is a function of position inside the bunch. In our case magnetic field value H_0 in the longitudinal center of the bunch at its boundary can be estimated

$$H_0 \cong \frac{4\pi}{c}\frac{eNc}{2\pi\sigma_x\sigma_b} \approx 2.8\cdot 10^{10}\ G,$$

so even for E =300 GeV, $\gamma \cong 6\cdot 10^5$, $Y_0 \cong 760$.

Radiation from interaction region.

Let us examine the conditions for radiation from IP. The formation length for the boundary particles goes to $l_F \cong \frac{\lambda\!\!\!^{-}_C\gamma}{Y_0^{2/3}\sigma_b}$. As the critical frequency of radiated photons goes to $\omega_c \cong mc^2\gamma/Y_0\hbar$, the corresponding wavelength goes to $\lambda\!\!\!^{-}_{cr} \cong c/\omega_c = cY_0\hbar/mc^2\gamma$. So the transverse size of coherence goes to $\sigma_\perp^{coh} \cong \sqrt{\lambda\!\!\!^{-}_{cr} l_F\sigma_b} = \sqrt{\frac{cY_0\hbar}{mc^2\gamma}\frac{\lambda\!\!\!^{-}_C\gamma}{Y_0^{2/3}}} = Y_0^{1/6}\lambda\!\!\!^{-}_C \sim 3\lambda\!\!\!^{-}_C \cong 1.15\cdot 10^{-10} cm$. The transverse dimensions of the bunch at IP, according to estimations are $\sigma_x \cong 1.1\cdot 10^{-9} cm$, $\sigma_y \cong 1.4\cdot 10^{-10} cm$, what is about the size of coherence.

14. MULTI-BUNCH OPERATION MODE

As the length of the laser spot on the structure is $l_f \cong L/N_R$, what means that in principle, that the number of the bunches could reach

$$N_B \cong l_f/\lambda \cong L/N_R\lambda.$$

Substitute here the numbers one can obtain $N_B \le 300$ for $\lambda \cong 1\mu\ m$, and $N_B \le 100$ for $\lambda \cong 10\mu\ m$. Of cause the real number of the bunches is less due to the raise/decrease finite time.

Using a train of bunches (up to 100, see above) one can decrease the number of the particles in each bunch and/or to increase the cross section of the beam, thereby allow some reasonable losses. The length of the laser spot at the structure is about $l_f \cong L/N_R$, what we estimated in section 9 as $l_f \approx 0.03 cm$ what is $\approx 30\lambda$ for $\lambda \cong 10\mu\ m$ and $\approx 300\lambda$ for $\lambda \cong 1\mu\ m$. As the $Q_{RF} \cong 9$ required, the bunch number could be up to 30. If collision arranged for few bunch

per train, N_B, then the luminosity will get a gain factor up to 30 also. These factors will allow increasing the transverse cross section and reducing the problems with radiation at IP. The H_B value required detailed considerations.

Multi-bunch structure could be arranged in a damping ring, in principle, with FEL methods. Using a laser with the same wavelength as required by acceleration structure and a dipole wiggler with period $\lambda_W \cong \lambda \cdot 2\gamma^2/(1+K^2)$, one could arrange an effective voltage $V \cong EKL_W/\gamma$, where E –is laser field strength. Then the bunching could go with usual autophasing regime. For example if $E \cong 1 MV/cm$, $\gamma \approx 10^3$ (500 *MeV*), $L_W \approx 20m$, then effective voltage could reach $V \cong 2\,MV$. Harmonics number (see Chapter 7) could reach $q \approx \Pi/\lambda \approx 10^5 \div 10^6$, where Π –is perimeter of the cooler. This is equivalent to $2GeV$ of fundamental accelerating RF (q=*1*).

15. ALIGNMENT

If the accelerating section is tilted on angle $\Delta\vartheta$ then the particles obtain the transverse momenta $\sim \Delta p_\perp \cong \Delta p_\parallel \cdot \Delta\vartheta$, where $\Delta p_\parallel$ –is an energy gain per section. Let us find the highest allowable value for the angle $\Delta\vartheta$. Ratio of the random component of transverse momentum per stage $\Delta p_\perp$ to the *full* momenta $p_\parallel$ must be less if compared with angular spread in the beam

$$\frac{\Delta p_\perp}{p_\parallel} << \sqrt{\frac{(\gamma\varepsilon)}{\beta\gamma}}\,.$$

The last yields

$$(\Delta\vartheta)^2 \equiv (\frac{\Delta p_\perp}{\Delta p_\parallel})^2 << \frac{\varepsilon}{\beta}(\frac{p_\parallel}{\Delta p_\parallel})^2 \equiv \frac{\varepsilon}{\beta}(\frac{\gamma}{\Delta\gamma})^2 \equiv \frac{\gamma\varepsilon}{\gamma\beta}(\frac{\gamma}{\Delta\gamma})^2 \equiv (\Delta\vartheta)^2_{beam}(\frac{\gamma}{\Delta\gamma})^2,$$

where $(\Delta\vartheta)^2_{beam} \cong \gamma\varepsilon/\gamma\beta$ is a squared angular spread in the bunch.

Substitute here extreme $\gamma\varepsilon_y \cong 2\cdot 10^{-9}\,cm\ rad$, $\gamma\varepsilon_x \cong 2.5\cdot 10^{-8}\,cm\ rad$, $\beta \cong 1\ cm$, $\gamma \cong 4000$ ($E \cong 2GeV$, at the beginning of acceleration), $\Delta\gamma \equiv 200$ for $\lambda_{ac} \cong 10\mu m$, $\Delta\gamma \equiv 2000$ for $\lambda_{ac} \cong 1\mu m$, and for the accelerating structure of 3 *cm* long one can obtain for $\lambda_{ac} \cong 10\mu m$ the allowable tilt of the order of

$$(\Delta\vartheta)^2_y << \frac{\gamma\varepsilon}{\gamma\beta}(\frac{\gamma}{\Delta\gamma})^2 = \frac{2\cdot 10^{-9}}{2\cdot 10^3}(\frac{4\cdot 10^3}{200})^2 = 4\cdot 10^{-10}, \text{ or } \quad \Delta\vartheta_y \cong 2\cdot 10^{-5}$$

$$(\Delta\vartheta)^2_x << \frac{\gamma\varepsilon}{\gamma\beta}(\frac{\gamma}{\Delta\gamma})^2 = \frac{2.5\cdot 10^{-8}}{2\cdot 10^3}(\frac{4\cdot 10^3}{200})^2 = 5\cdot 10^{-9}, \text{ or } \quad \Delta\vartheta_x \cong 7\cdot 10^{-4}$$

For $\lambda_{ac} \cong 1\mu m$ these numbers is ten times less. These numbers yield that the ends of 3*cm* long structure must be aligned better that 0.6 micrometers for vertical and 21 micrometers for radial directions.

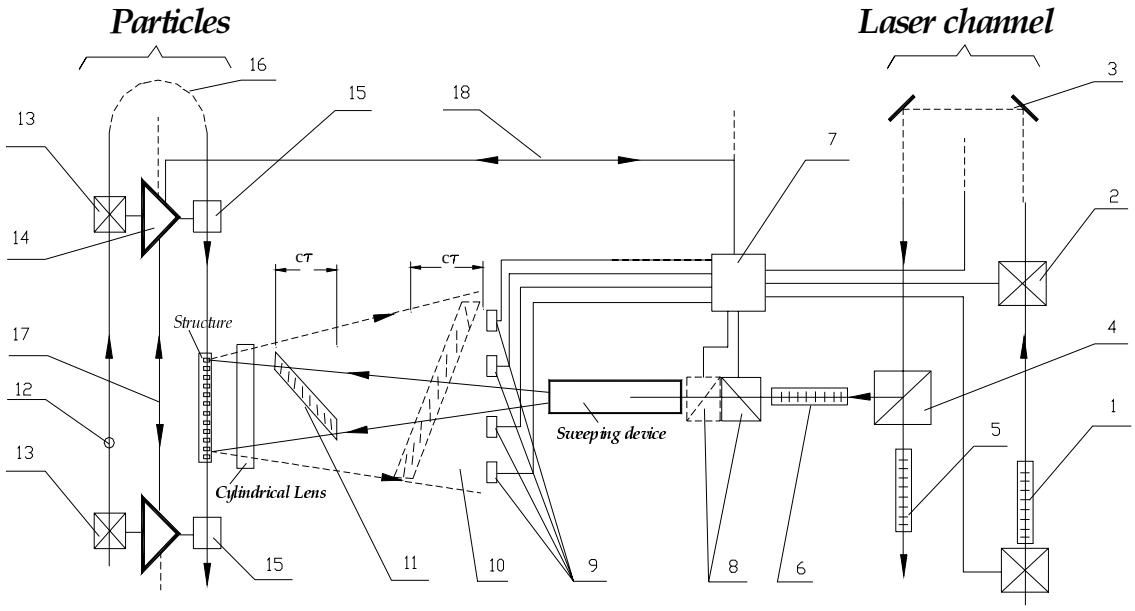

FIG

FIGURE 34: Schematic view on the feedback system fragment. On the right the optical part and on the left the beam part represented respectively. 1–is a driving laser bunch, 2–is transverse position sensor for a laser bunch, 3–is a laser back reflector loop, 4 –is a power splitter, 5–is a driving bunch on the way to next module, 6–is a splitted part of driving laser bunch, 7–is a processor, 8–are the beam deflectors for two transverse directions, 9–is an array of optical sensors, 10–is a reflected laser bunch, 11–is a sweeped laser bunch. 12–is an electron/positron bunch on the way to the beginning of accelerator. 13–are the pick up electrodes, 14–is a functional amplifier, 15–is a transverse kickers, 16–is a beam back returning loop, 17,18 –are the lines of the signal processed. Lines across the laser bunch indicate the wavefronts. The back loop 3 located at the beginning of accelerator (acceleration process).

16. GENERAL PICTURE

TLF method promises up to 30 *TeV/km* or 300 *TeV* on 10 *km* with 0.3 *J/m* or with 3 *kJ* per pulse total. So the total output power of the laser must be within 5 *MW/10km* with repetition rate about 160 *Hz* for $\lambda \cong 1\mu m$.

The gradients still far below the *absolute* limit of the acceleration gradient, what is defined by Schwinger field , $E^{\infty} \cong 2.6 \cdot 10^{9}\, GeV/m$, or $2.610^{10}\, TeV$ on 10*km*.

Simplified view of such an assembly is represented in Fig. 35 below. All elements are installed in vacuumed volume, not shown in this Figure.

Primary laser beam 1 goes to the end of accelerator. Mirrors 2 redirect it back, pos.3, trough the sequence of splitters. In the similar way the particle's beam 5, goes trough bending system 6 and further trough structures to next modules, 4. 7 and 8 –are the focusing elements for the laser and particle's beam respectively. Optical platform 9 is standing on legs 10 with active damping system to minimize vibrations. 13–cylindrical lenses, 14–are the accelerating structures. All elements on the table are located in a vacuumed volume, not shown here.

The direction of the accelerating structures as indicated in Fig. 15.1 helps to run the elecron/positron bunch through the structures, as in horizontal plane the corresponding emittance is bigger. For ion/meson beams this advantage is not used.

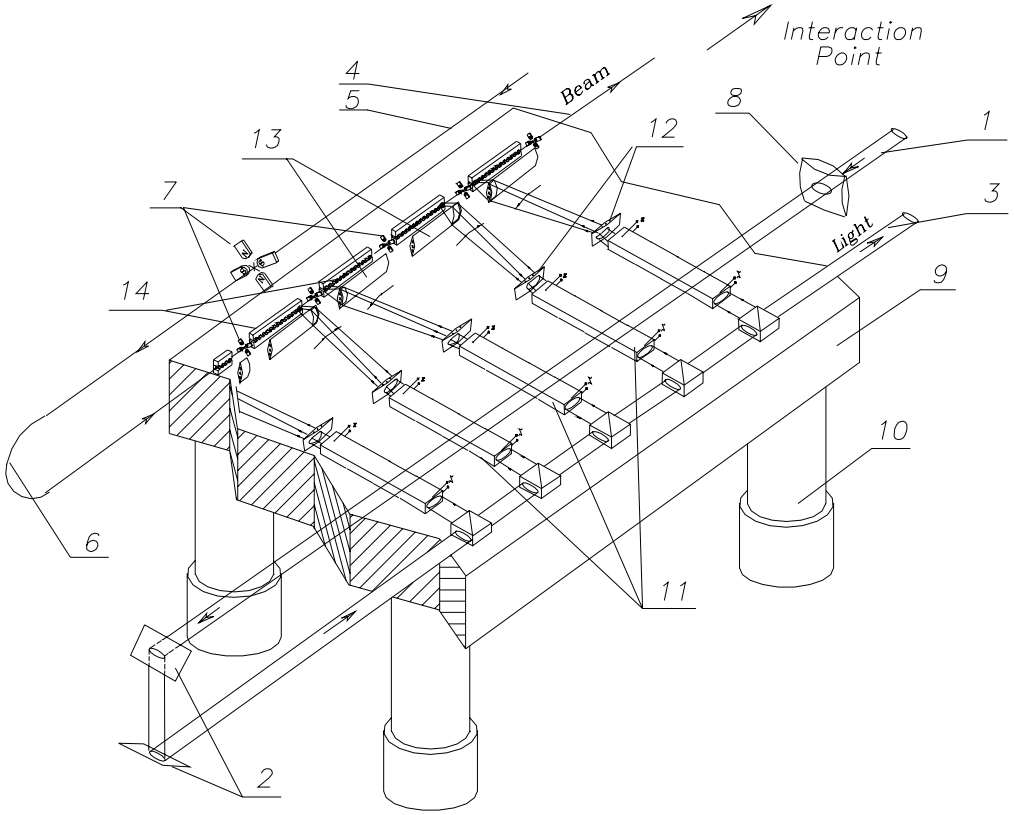

FIGURE 35: All elements installed on a platform (9). The direction of largest emittance in damping ring (horizontal, if wigglers have vertical magnetic field) is now going along the passing slots in structure. This helps to keep emittance low during acceleration. Light means laser beam. Other comments are in the text.

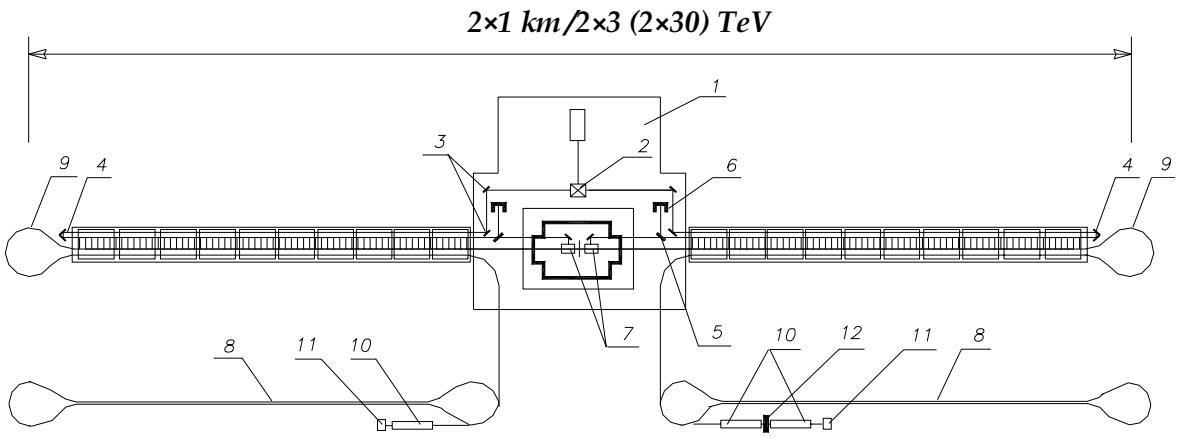

FIGURE 36: Laser Linear Collider (LLC) complex. 1–is a laser master oscillator platform, 2 –is an optical splitter, 3,4–are the mirrors, 5–is a semi-transparent mirror, 6–is an absorber of laser radiation. 7–are the Final Focus Systems. 8–are the damping systems for preparing particle's beams with small emittances, 9–are the bends for particle's beam. 10–are the accelerating X-band structures, 11–is an electron gun, 12–is a positron converter. The scheme with the damping rings as sources are shown here.

TABLE 1. Parameters of the Laser Linear Collider.

Parameter	$\lambda_{ac} \cong 10\mu m$	$\lambda_{ac} \cong 1\mu m$
Energy of $e^{\pm}$ beam	3×3 *TeV*	30×30 *TeV*
Total two-linac length	2×1 *km*	2×1 *km*
Main linac gradient	3 *GeV/m*	30 *GeV/m*
Luminosity/bunch	$10^{34} cm^{-2} s^{-1}$	$10^{34} cm^{2} s^{-1}$
No. of bunches/pulse	$10\ (\leq 100)$*	$30\ (\leq 300)$*
Laser flash energy/Linac	300*J*	300*J*
Repetition rate	160 *Hz*	160 *Hz*
Beam power/Linac	2.3 *kW*	760*W*
Bunch population	10^{7}	10^{6}
Bunch length	$1\mu m$	$0.1\mu m$
$\gamma \varepsilon_x$ / $\gamma \varepsilon_y$	$\approx 10^{-8} / 10^{-9}$ *cm·rad*	$5 \cdot 10^{-9} / 1 \cdot 10^{-10}$ *cm·rad*
Damping ring energy	2 *GeV*	2 *GeV*
Length of section/Module	3*cm*	3*cm*
Wall plug power**	2×0.5 *MW*	2×0.5 *MW*

*–Maximal possible number. **–Laser efficiency $\approx 10\%$. The power for supplemental electronics is not included.

General view of Linear Laser Collider complex for 2x200 GeV

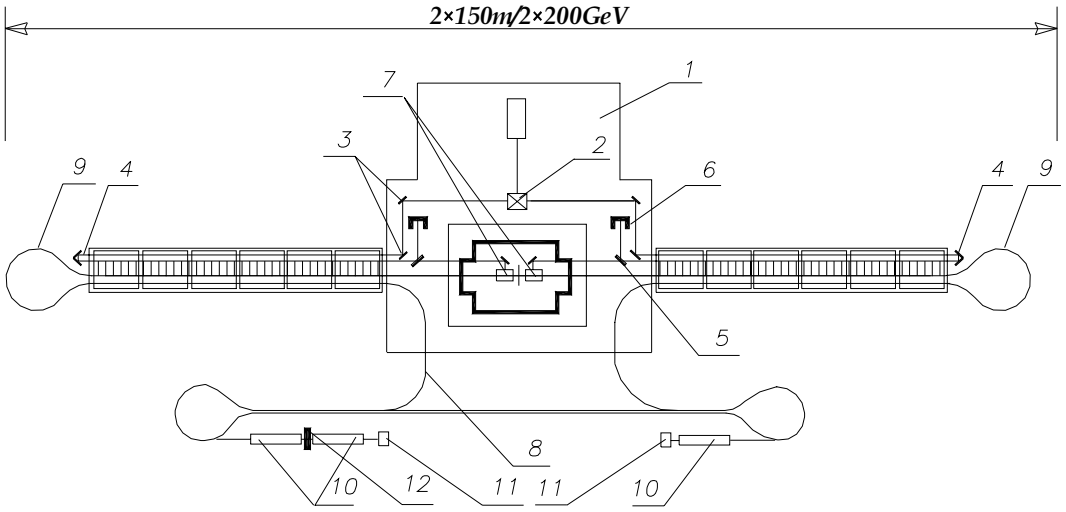

FIGURE 37: Laser Linear Collider (LLC) complex. 1–is a laser master oscillator platform, 2 –is an optical splitter, 3,4–are the mirrors, 5–is a semi-transparent mirror, 6–is an absorber of laser radiation. 7–are the Final Focus Systems. 8–are the damping systems for preparing particle's beams with small emittances, 9–are the bends for particle's beam. 10–are the accelerating X-band structures, 11–is an electron gun, 12–is a positron converter. The scheme with the damping rings as sources are shown here.

TABLE 2. Parameters of the Laser Linear Collider for $200 \times 200\ GeV$.

Wavelength	$\lambda_{ac} \cong 1\mu m$
Energy of $e^{\pm}$ beam	$200 \times 200\ GeV$
Total two-linac length	$2 \times 200\ m$
Main linac gradient	$1.2\ GeV/m$
Luminosity/bunch	$10^{32} cm^{-2} s^{-1}$
No. of bunches/pulse	$10\ (\leq 100)$
Laser flash energy/Linac	$3J$
Repetition rate	$160\ Hz$
Beam power/Linac	$5\ W$
Bunch population	10^5
Bunch length	$0.1\ \mu m$
$\gamma\varepsilon_x\ /\ \gamma\varepsilon_y$	$\approx 10^{-8}/10^{-9}\ cm \cdot rad$
Damping ring energy	$2\ GeV$
Disruption parameter	1.4
Length of section/Module	$3cm$
Wall plug power	$2 \times 5kW$

17. PERSPECTIVES AND APPLICATIONS

Feasibility of $\mu^+\mu^-$, $\pi^+\pi^-$, $\pi p, \mu p$ and ion-ion collisions. Table-top machineS

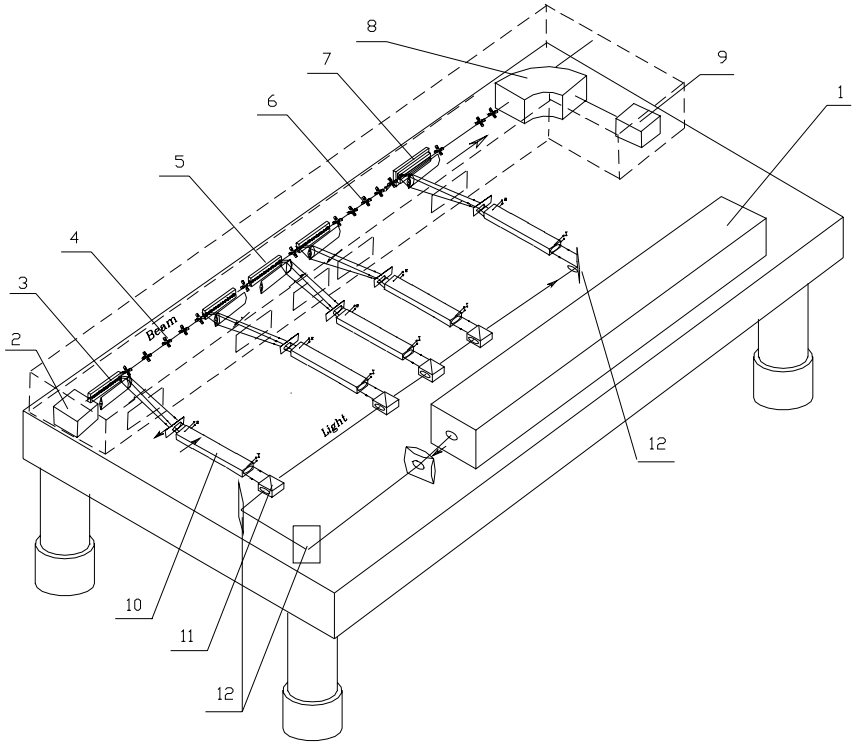

FIGURE 38: 100 MeV accelerator with a Compton wiggler concept. All elements installed on a platform. Light means laser beam. Other comments are in the text. Vacuumed cover for the beam part is shown in dashed lines. 1 –is a laser, 2–is source of particles, including micro-tip and movers, 3–RF prebuncher, 4–ias a space for buncher (if necessary) and beam longitudinal structure formation, 5–is main acceleration modules, 6–focusing elements, 7–a region for laser wiggler, 8–bending magnet, 9–is beams dump, 10–is a sweeping device, 11–is a splitting device, 12–is a mirror.

TABLE 3. Parameters of the laser-driven tabletop linac.

Wavelength	$\lambda_{ac} \cong 1\mu m$
Energy of $e^{\pm}$ beam	100 *MeV*
Active linac length	10 *cm*
Main linac gradient	1.0 *GeV/m*
Bunch population	10^6
No. of bunches/pulse	10 (≤ 100)
Laser flash duty	100 *ps*
Laser flash energy	*5mJ*
Repetition rate	160 *Hz*
Average laser power	~0.8*W*
Average beam power	26 *mW*
Bunch length	0.1 μm
$\gamma\varepsilon_x$ / $\gamma\varepsilon_y$	$\approx 10^{-8}/10^{-8} cm \cdot rad$
Length of section/Module	3*cm*
Wall plug power	3.5*kW*

18. CONCLUSION

Combination of words –"Laser Acceleration" – probably expels interest, rather than attracts it because of extremely heavy history.
Laser people undermined the subject significantly in the minds.
Second disastrous wave arrived from plasma physics.

It is time to accept for accelerator physicists, that the new ***micro–technology*** available, opens new possibilities for accelerator physicists themselves. This new technology opens new approaches to accelerator physics at all. Accelerator physicists and engineers need to study this new subject from the beginning. Now there is no necessity for huge infrastructure to make a high-energy accelerator, as it could be located in average room now practically at any University. Moreover, the financing of a laser driven accelerator project is now available for private companies.

And when the new method will bring success, it will be easy to arrange collisions with μ, π, p, *ion-ion* (and what ever) naturally and cheaper.

Higher gradients required not only as a desire to make accelerator more compacted but as a vital necessity to accelerate amount of particles, necessary to obtain a reasonable luminosity. As the scale goes down, the wakes grow even faster and the only way to keep the proper ratio of wakes to accelerating field –to make the last one as big as possible.
Second is that any point of accelerating structure must be illuminated for the minimal time in order to avoid the damage associated with the overheating.
***Traveling Laser Focus, TLF*- method solves most of the problems in acceleration.**
For a $0.5 \times 0.5\, TeV$ Collider the total length becomes $2 \times 170\ m$ for $\lambda_{ac} \cong 10 \mu m$ and $2 \times 17\ m$ for $\lambda_{ac} \cong 1 \mu m$ respectively with $0.3 J/m$ feeding power. One can compare these numbers with that from Linear Collider projects, which are under consideration in few Laboratories around the World ($2 \times 10\ km$ gives the same $2 \times 0.5\ TeV$). With TLF approach, main investments are going into *new technology*, what in any case will serve in a future.

As this is not prohibited by quantum mechanics, the emittances could reach its lowest values $\gamma\varepsilon_x \gamma\varepsilon_y \gamma\varepsilon_s \geq \lambda\!\!\!^{-3}_C N$.

The TLF method could be staged very well with clear results after each stage completed. One stage may include fabrication and cold testing of accelerating structures. Small power lasers could be used for these purposes. This will include exercises on alignment, tuning and fabrication experience. Other stage includes development and test of the sweeping device. The low emittance solid-state electron or ion source might be another stage for this job.

At the end we can conclude, that the problem of acceleration in a laser-driven linac could be reduced with TLF method to a present day technology.